6
High Performance Flexible RRAM Devices for Multilevel Resistive Switching

This chapter investigates the development of flexible RRAM devices using a PVP:$MoSe_2$ composite as the switching layer, achieving high-performance resistive switching with low operating voltages (0.7 V/-1 V). The devices exhibit forming-free behavior, multilevel data storage with a high I_{ON}/I_{OFF} (~10^3), and excellent reliability, including retention up to 10,000 seconds and endurance exceeding 1,000 cycles. Mechanical stability is demonstrated under bending conditions, maintaining functionality at radii as small as 7 mm. These results with PVP:$MoSe_2$ composite switching layer is a promising candidates for next-generation flexible and high-density memory applications are recently published in [Saini et al., 2024].

6.1 Introduction

The demand for lightweight, wearable, flexible, and robust memory storage technologies has recently increased due to the surge in interest of new applications in flexible and wearable electronics [Lee et al., 2024]. Due to properties such as ease of fabrication and large-area applicability, RRAM devices have become an emerging choice for data storage for flexible electronics [Rao et al., 2023]. The switching performance of a RRAM device depends on the switching material as well as the top and BEs [Kumar et al., 2023]. Though the choice of electrodes to be explored is limited, various categories of switching materials are being explored for flexible RRAM devices, which include various organic polymers, TMOs, and various 2-D materials such as GO, carbides and nitrides of transition metals (MXenes), and TMDs [Biswas et al., 2021, Kumar et al., 2020, Zhang et al., 2017, Park et al., 2024]. TMOs such as HfO_x, TiO_x, and AlO_x, had been extensively explored for CMOS technology, which gave them an added advantage of availability and established material properties [Yan et al., 2019]. Though TMOs show high potential as a switching layer due to excellent film qualities [Wong et al., 2012], the rare disadvantages such as high processing temperature and lack of mechanical flexibility, which limits their utilization in fabrication of flexible electronic devices [Lanza et al., 2019]. The other promising categories of materials for flexible RRAMs are polymers such as PVPy, PVP, and PVK, which can help in adding low-temperature processing ability and mechanical flexibility [Dlamini et al., 2022, Ali et al., 2017, Saini et al., 2023]. These materials inherently have mechanical flexibility and are eco-friendly and mostly solution processed, leading to overall low cost [Yang et al., 2023]. The resistive switching in the polymers can be attributed to formation and rupture of metallic or carbonaceous filaments [Lee et al., 2015]. Two-dimensional materials have gained tremendous attention recently, and their exploration for resistive switching has become a major research area [Park et al., 2022, Chen et al., 2020]. Among various 2-D materials, GO is one of the earliest and most widely explored materials in RRAM devices [Varun et al., 2020, Wang et al., 2012]. It has also been explored in bilayer combination with polymers like PVA, which improved the device performance, as the presence of abundant oxygen-containing functional groups on the surface of GO can form hydrogen bonds with the hydroxyl groups and thus form a stable and uniform solution [Chen et al., 2022]. The other set of explored 2-D material families for resistive switching are MXenes, where M represents transition metals and X represents carbides or nitrides; [Ding et al., 2019] however these materials require complex steps in the synthesis process like multiple etching with acids and are in the initial stage of their exploration [Feng et al., 2023]. In addition, TMDs like MoS_2, WS_2, $MoSe_2$, andWSe_2 are aggressively being explored as switching layers in flexible RRAM devices, owing to the excellent mechanical strength along with the advantage of tunability of properties like thickness, energy band gap, inter layer distance interfacing, and chemical structure [Kumar et al., 2019, Shen et al., 2023, Rehman et al., 2016]. MoS_2 has been

widely explored in composite form with various other materials such as ferroelectrics, metal nanoparticles, and organic polymers to demonstrate flexible RRAM devices with decent switching performance and bendability [Zhang et al., 2016]. $MoSe_2$ is another important material of the TMD family that has shown decent resistive switching behavior though mostly reported through RRAM devices on rigid substrates as pristine, through rarely explored in flexible RRAM devices [Zhang et al., 2016, Saini et al., 2023]. $MoSe_2$ is also investigated as a switching layer in composite with polymers such as PMMA and PVA in hybrid bilayer combination with TiO_2, again on rigid substrates [Wang et al., 2019]. One more versatile polymer candidate for composites with these 2 D materials can be PVP due its high dielectric constant, mechanical flexibility, and excellent film forming properties [Sun and Wen, 2019, Varun et al., 2020], however, it is not investigated as a composite with $MoSe_2$ to date, to the best of our knowledge. Moreover, it is difficult to find any report on investigation of $MoSe_2$ in composite form as a switching layer for demonstration of high-performance RRAM devices, which is surprising considering the significant potential of this material as a switching candidate.

6.2 Fabrication of Ag/$MoSe_2$:PVP/ITO Flexible RRAMs

Flexible RRAM devices were fabricated on a PET substrate coated with conducting ITO, where ITO was taken as the BE. PET substrates were cleaned by using ultrasonication in methanol and IPA followed by nitrogen drying. PVP (Mw =25000) and $MoSe_2$ (325 mesh) were procured from Sigma-Aldrich Inc. The first solution was prepared using 2.5 wt% PVP in IPA solvent for a 30 minutes ultrasonication. The second solution was prepared with $MoSe_2$ in methanol by a liquid exfoliation method [Saini et al., 2023]. For the same 4 mg/mL solution was ultrasonicated (around 90%) and centrifuged for 30 minutes at 4000 rpm. Again, the upper part of the supernatant was deposited over BE. Next to make the final composite of PVP and $MoSe_2$, both solutions were mixed in a 4:1 ratio and sonicated for 30 minutes to dissolve properly. All three solutions were spin-coated over BE at 2000 rpm for 45 seconds. Samples were annealed at 100 °C for 1 hour to remove the residual solvent.

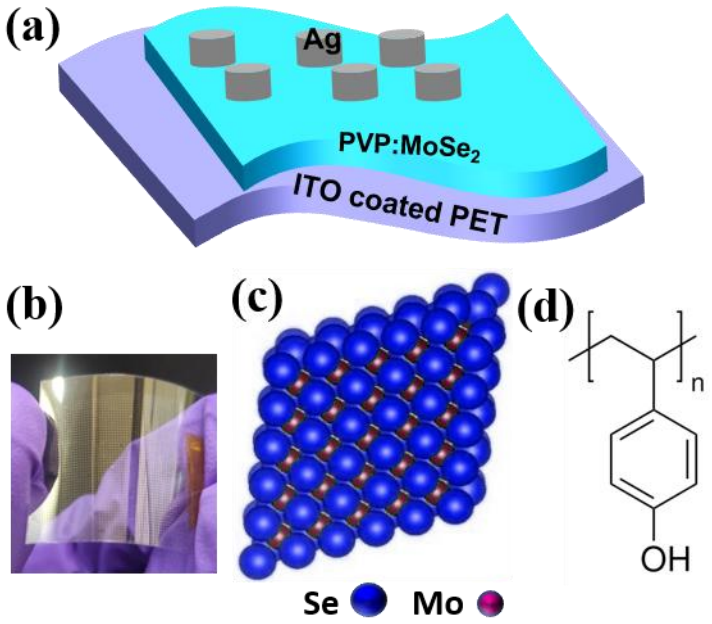


Figure 6.1 (a) Schematic structure and **(b)** digital picture of fabricated Ag/PVP:$MoSe_2$/ITO flexible RRAM device. Chemical structure of $MoSe_2$ **(c)** and PVP**(d).**

Finally, using thermal evaporation under high vacuum of 1.2×10^{-6} Torr, the circular Ag TE with a 100 µm diameter were deposited using a shadow mask. A Keithley 4200 SCS was used for the electrical characterization of the devices. Raman spectra of the $MoSe_2$ film were carried out by the Bay Spec system. Figure 6.1(a & b) show the schematic structure and digital image of

Ag/PVP:$MoSe_2$/ITO flexible RRAM device. The chemical structure of $MoSe_2$ and PVP are shown in Figure 6.1(c & d) respectively.

6.3 Results and Discussion

6.3.1 Surface Morphology and Material Characterization

The Raman spectrum of $MoSe_2$ film on a glass substrate is shown in Figure 6.2(a). A sharp Raman peak is obtained at 243 cm^{-1}, which indicates the A_1g mode (out-of-plane vibration) in the exfoliated thin film over a glass substrate and thus proves the presence of $MoSe_2$ nanoparticles in the film [Liu et al., 2018]. Figure 6.2(b) shows the Tauc plot of $MoSe_2$ obtained by UV–visible fluorescence spectroscopy. The Tauc plot, a widely acceptable method for evaluation of the energy gap (E_g), is a graph plotted with $(\alpha\hbar\nu)^2$ on the y-axis and $(\hbar\nu)$ on the x-axis where α is the absorption coefficient, $\hbar$ indicates the Plank constant, and ν is the frequency. In Figure 6.2(b), E_g of $MoSe_2$ is calculated from the slope of the Tauc plot by extrapolating the slope, and an E_g of ~1.4 eV is observed. The AFM images of the top surface of PVP, $MoSe_2$, and PVP:$MoSe_2$ films with a depth variation bar are shown in Figure 6.2(c), (d), and (e), respectively. The corresponding root-mean-square values of roughness (R_q) were obtained to be 0.55, 10.34, and 4.25 nm, respectively. It can be observed that, as expected, a smoother film has been obtained in the case of the composite when compared to pristine $MoSe_2$, which is desirable for further device fabrication.

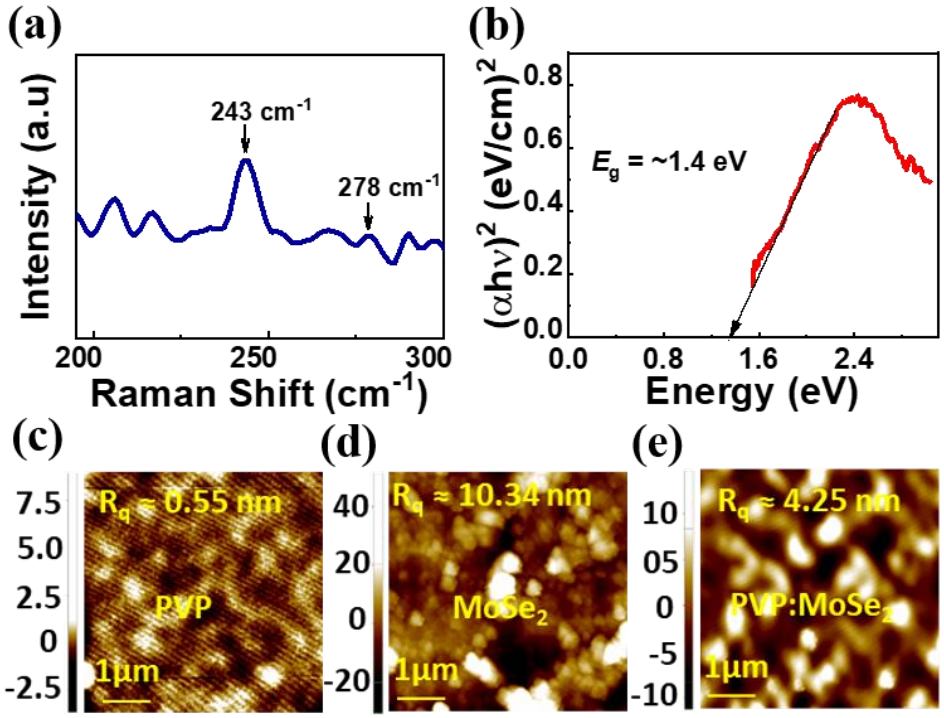


Figure 6. 2 (a) Raman characteristics and **(b)** Tauc's plot of $MoSe_2$ thin film. AFM image of **(c)** PVP, **(d)** $MoSe_2$, and **(e)** PVP:$MoSe_2$ thin film.

6.3.2 Electrical Performance of Flexible RRAMs

Current–voltage (I–V) characteristics of flexible RRAM devices with pristine (PVP, $MoSe_2$), and nanocomposite (PVP:$MoSe_2$) active layers were obtained by applying a linear voltage sweep from 0 → V_{max} → 0 with a 1 mA compliance current for SET and 0 → $-V_{max}$ → 0 without a compliance current limitation for RESET. The compliance current during the SET cycle is required to protect the device from damage or burnout due to excessive current flow. The I–V characteristics of PVP, $MoSe_2$, and PVP:$MoSe_2$ of the first cycle are shown in Figure 6.3(a , b & c) respectively. It can be clearly seen from the plot that all three devices exhibit bipolar resistive switching behavior. It was observed that the switching window was very small with very low I_{ON}/I_{OFF} (~10) for the devices with a pristine PVP active layer.

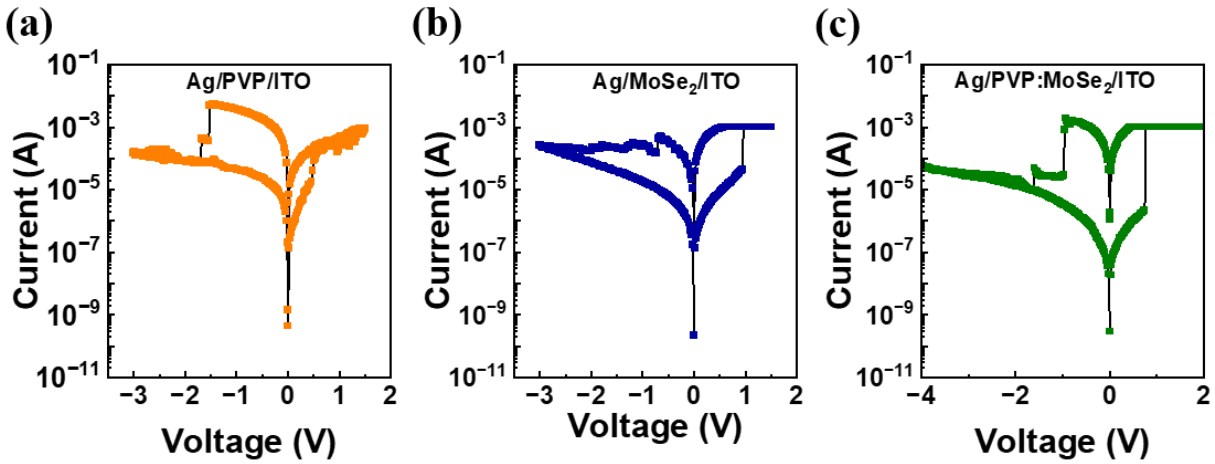


Figure 6.3 *I–V* characteristics of PVP **(a),** $MoSe_2$ **(b),** and PVP:$MoSe_2$ **(c),** respectively.

The corresponding SET/RESET switching voltages were ~1 V/–1.5 V. Better switching behavior was observed for devices with a pristine $MoSe_2$ active layer, with a lower SET/RESET voltage of 1 V/–1.2 V possibly due to better conductivity of the $MoSe_2$ layer due to a smaller band gap. In Figure 6.3(c), it can also be seen that devices with the composition of PVP:$MoSe_2$ exhibited better switching characteristics with a higher memory window than devices with pristine PVP or $MoSe_2$ as the active layer. Moreover, lower SET and RESET voltages of 0.7 V and −0.9 V, respectively, were observed. To check the device-to-device variability, six devices were randomly chosen from particular substrates of devices with PVP, $MoSe_2$, and PVP:$MoSe_2$ active layers, and *I–V* characterizations were performed at a 1 mA compliance current as shown in Figure 6.4(a), (b), and (c), respectively.

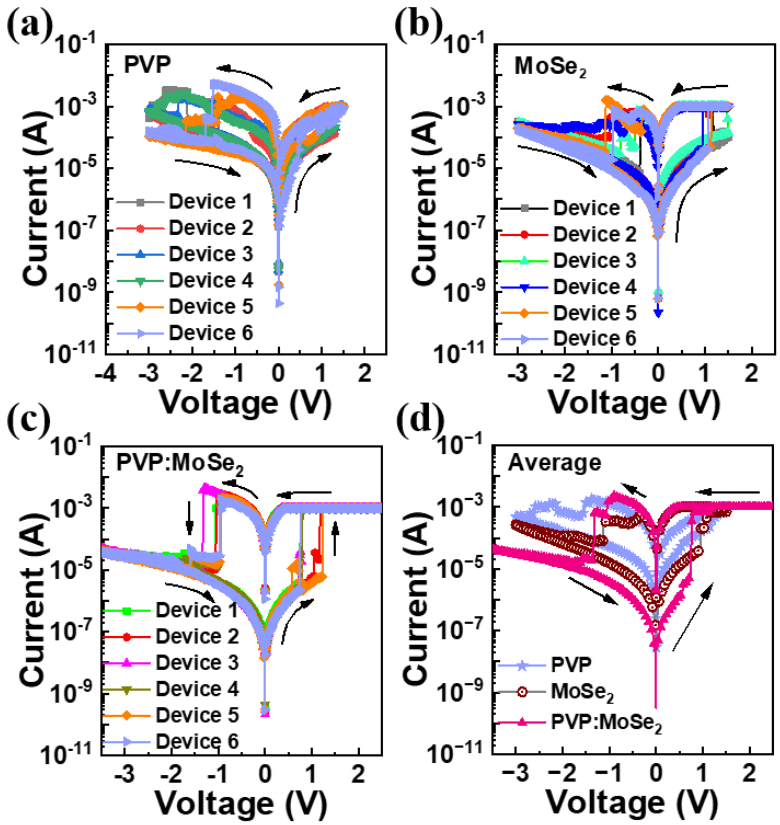


Figure 6.4 *I–V* characteristics of six randomly chosen devices from the same substrate of PVP **(a),** $MoSe_2$ **(b),** and PVP:$MoSe_2$ **(c),** respectively, to investigate the device-to-device variation, and average *I–V* characteristics of those six devices for all three cases **(d).**

The stochastic nature of filament formation and rupture in RRAM devices leads to the cycle-to-cycle and device-to-device variation in *I–V* characteristics. The composite of $MoSe_2$ with PVP reduces the device-to-device variation in comparison to neat PVP or $MoSe_2$ active material RRAM devices. The device-to-device variability in switching performance was quantitatively investigated and compared for flexible RRAM devices with PVP, $MoSe_2$, and PVP:$MoSe_2$ active layers, specifically with respect to V_{SET}/ V_{RESET} and I_{ON}/I_{OFF}. The same is summarized in Table 6.1 with average and standard deviations for all cases. It can be clearly seen from these results that the I_{ON}/I_{OFF} and V_{SET}/ V_{RESET} variation is very low in the flexible RRAM device with a PVP:$MoSe_2$ active layer.

Table 6.1: Quantitative Comparison of Device-to-Device Variability in Flexible RRAM Devices with $MoSe_2$ in Pristine, Composite, or Bilayer Form

Active Layer	V_{SET} (V)	V_{RESET} (V)	I_{ON}/I_{OFF}
PVP	1.22 (± 0.30)	-1.86 (±0.50)	1.2×10^1
$MoSe_2$	1.14 (± 0.17)	-0.81 (±0.26)	2.3×10^2
PVP:$MoSe_2$	0.87 (± 0.30)	1.18 (± 0.30)	1.83×10^3

Additionally, the average of *I–V* characteristics of the six devices for each active layer (PVP, $MoSe_2$, and PVP:$MoSe_2$) are plotted in Figure 6.4(d). The average plot confirms the fact that the flexible RRAM devices with a PVP:$MoSe_2$ composite active layer exhibit better switching compared to devices with pristine PVP or $MoSe_2$ active layers. Flexible RRAM devices with a PVP:$MoSe_2$ active layer were further investigated for switching performance, which includes exploration for multilevel storage, cycle-to-cycle variation, conduction mechanism, and mechanical stability for the reliable and stable RRAM device operation. Multilevel switching is the simplest way to accommodate more data information at low cost for the applications of high-density storage [Ling et al., 2017]. In RRAM devices, the multilevel switching can be controlled in three ways, by modulating the compliance current, by changing the RESET voltage, and by varying the pulse width of the write/erase operation [Zahoor et al., 2020, Zhou et al., 2024]. Among them modulation of the compliance current can be an easy and effective way to investigate the functionality of multilevel resistive switching [Wang et al., 2022, Tsigkourakos et al., 2017]. Flexible RRAM devices with a PVP:$MoSe_2$ active layer were explored for multilevel resistive switching by utilizing the three distinct compliance current values of 100 µA, 500 µA, and 1 mA, as shown in Figure 6.5.

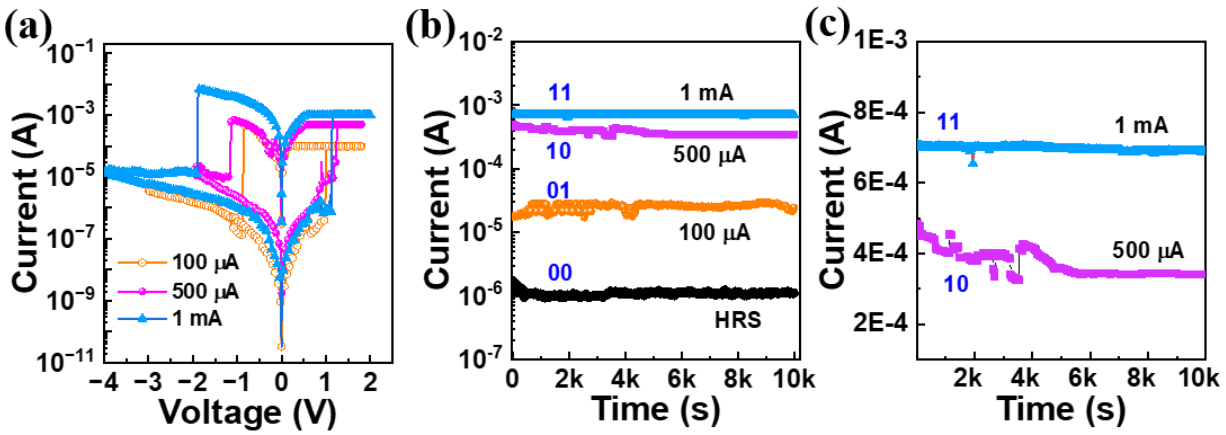


Figure 6.5 Exploration of multilevel switching through I–V characteristics **(a)** and retention time **(b)** of the Ag/PVP:MoSe2/ITO RRAM device by variation of the compliance current. **(c)** Retention time plot of Ag/PVP:$MoSe_2$/ITO RRAM device for '10', and '11' state in the current range of 100 µA to 1 mA.

The *I–V* characteristics for the same is shown in Figure 6.5(a). The HRSs are very close for each compliance current, and LRSs change as compliance current changes. Thus, the HRS can be considered as a '00' state, and the other three LRSs are considered as '01', '10', and '11' data states. Retention time characterization was performed by applying a read voltage of 0.2 V with compliance free conditions to check the stability of the multilevel storage of the RRAM device. The value of the read voltage was chosen in such a way that it does not change the current state of the device. The retention plot for 100 µA, 500 µA, and 1 mA compliance currents for 10^4 seconds at the read voltage of 0.2 V is plotted in Figure 6.5(b). The LRS currents for 100 µA, 500 µA, and 1 mA compliance currents are 24.6 µA, 338 µA, and 689 µA, respectively which are showing '01', '10', and '11' states. Distinct levels for '01', '10', and '11' data states can be clearly observed in this Figure, indicating that demonstration of 2-bit storage (00, 01, 10, and 11) is possible from these devices using four distinct states, which include one HRS and three LRSs. For more clarification, the retention time plot for '10', and '11'state in the current range of 100 µA to 1 mA in linear scale are plotted as shown in Figure 6.5(c). The endurances of these Ag/PVP:$MoSe_2$/ITO flexible RRAM devices for compliance currents of 1 mA, 500 µA, and 100 µA at a read voltage of 0.2 V are shown in Figure 6.6(a), (b), and (c), respectively. The LRS and HRS plots of 280, 280, and 1150 cycles are shown, respectively, for these three cases. As it can be seen in Figure 6.6(a) for a compliance current of 1 mA, the variation in LRS is larger than HRS at a higher compliance current, which may be explained by the behavior of filament formation. The devices with low compliance current (100 µA) show decent I_{ON}/I_{OFF} even after more than 1000 DC sweep cycles.

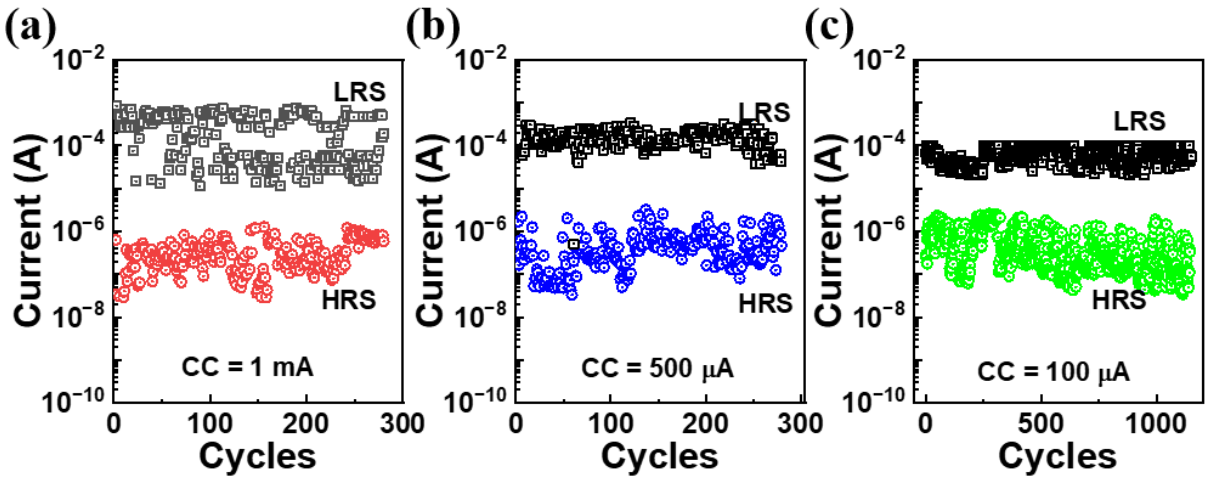


Figure 6.6 Endurance of Ag/PVP:$MoSe_2$/ITO flexible RRAM devices for compliance currents of 1 mA **(a),** 500 µA **(b),** and 100 µA **(c).**

6.3.3 Conduction & Switching Mechanism

The charge carrier transport mechanism in the fabricated flexible RRAM devices was investigated using double log(*I–V*) characteristics, as shown in Figure 6.7. The linear fitted *I–V* curve of double log(*I–V*) for positive voltage is depicted in Figure 6.7(a). The fitted curve with a slope value of 1 indicates the ohmic conduction ($I \propto V$) region at a low voltage. This is mainly due to partially filled traps inside the dielectric layer. At higher voltage, the current is limited by the SCLC described by Child's law, which clearly can be seen by the slope value ~2 ($I \propto V^2$) [Dwivedi et al., 2022]. As the applied voltage is increased after this point, a sudden jump in current can be observed that marks the shift in state of device from HRS to LRS, due to formation of a conducting filament. While retracting the positive voltage, a slope of 1 is observed with higher current, verifying the presence of the conducting filament and thus ohmic conduction [Saini et al., 2024]. The double log(*I–V*) of the negative voltage sweep is shown in Figure 6.7(b).

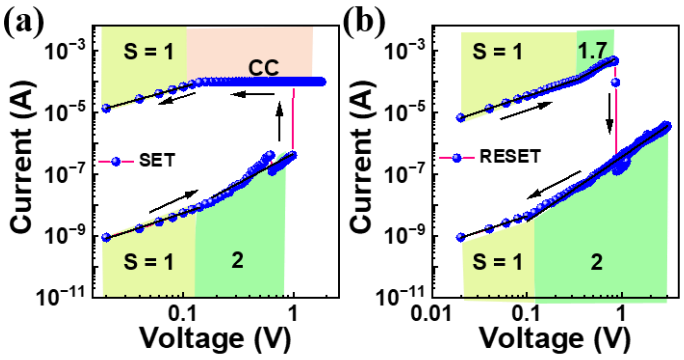


Figure 6.7 Double log *I–V* characteristics of Ag/PVP:$MoSe_2$/ITO flexible RRAM for SET **(a)** and RESET **(b).**

Similar to the positive voltage sweep, in the negative voltage sweep also a slope value of ~2 and 1.7 at higher voltage indicates the SCLC mechanism and a slope value of ~1 at lower voltages indicates ohmic conduction. The sudden fall of current indicates the RESET voltage and marks the shift of the device state from LRS to HRS. The fall in current is due to the rupture of the conducting filament that was formed during the SET cycle. The switching mechanism of Ag/PVP:$MoSe_2$/ITO RRAM devices for LRS and HRS are shown in Figure 6.8(a & b). When a positive bias (V_{SET}) is applied to the electrochemically active Ag TE with respect to the BE, it undergoes the oxidation process, which results in the ionization of Ag atoms to the Ag^+ ions that migrate toward the BE under the electric field. Simultaneously, electrons are injected from BE and move toward the TE. As these electrons approach the TE, the Ag^+ ions reduce these electrons to form Ag atoms, creating a conductive filament that forms a continuous path from the bottom to the TE, as shown in Figure 6.8(a). This process results in a significant increase in current, indicating the transition of the device from HRS to LRS. The RESET process is illustrated in Figure 6.8(b).

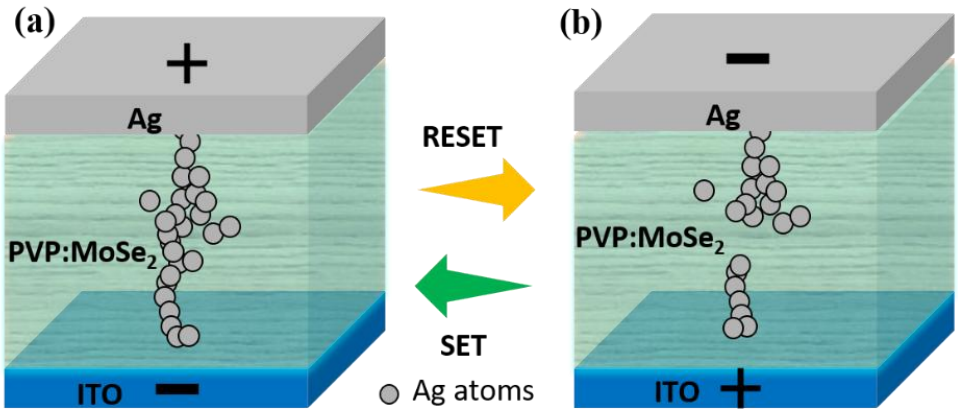


Figure 6.8 Schematic structure of the switching mechanism of Ag/ PVP:$MoSe_2$/ITO flexible RRAM for LRS **(a)** and HRS **(b).**

Now a negative bias (V_{RESET}) is applied across the TE and BE to reset the device to the HRS. This bias increases the current through the nanoscale filament, causing it to undergo Joule heating and ultimately break down. This breakdown facilitates the return of Ag^+ ions to the TE, where they are reduced back to Ag atoms [Saini et al., 2023]. Therefore, the conduction mechanism in Ag/PVP:$MoSe_2$/ITO RRAM devices is based on the filament formation and rupture where $MoSe_2$ acts as a charge-trapping site in the switching layer while the PVP avoids the leakage of the charge stored in the device. The charge storage is mainly due to the presence of $MoSe_2$ in the composite PVP:$MoSe_2$ switching layer [Kaur et al., 2022].

6.3.4 Charge Transport Mechanism

On the basis of the above observations, a schematic energy band diagram of physical charge transport in a Ag/PVP:$MoSe_2$/ITO flexible RRAM device is shown in Figure 6.9, without bias (a), with positive bias (b), and with negative bias (c), at the top Ag electrode. The PVP layer has a wider band gap (4 eV) in comparison to $MoSe_2$ (1.4 eV), and thus PVP acts as a charge-blocking layer, whereas $MoSe_2$ behaves as a charge-trapping material. Charge trapping is depicted in Figure 6.9(b). When a positive voltage sweep is applied across the TE and BE, injected charges get trapped, and at a certain voltage the device reaches its SET state [Das et al., 2021, Zhang et al., 2019]. Now when a negative voltage sweep is applied, the device migrates from the SET state to the RESET state with the charge transport mechanism as depicted in Figure 6.9(c). During the negative voltage sweep, the charge carrier that has been trapped in the $MoSe_2$ layer during the SET process get detrapped [Sarkar et al., 2015]. This trapping and detrapping of charge carriers will be repeated for every cycle.

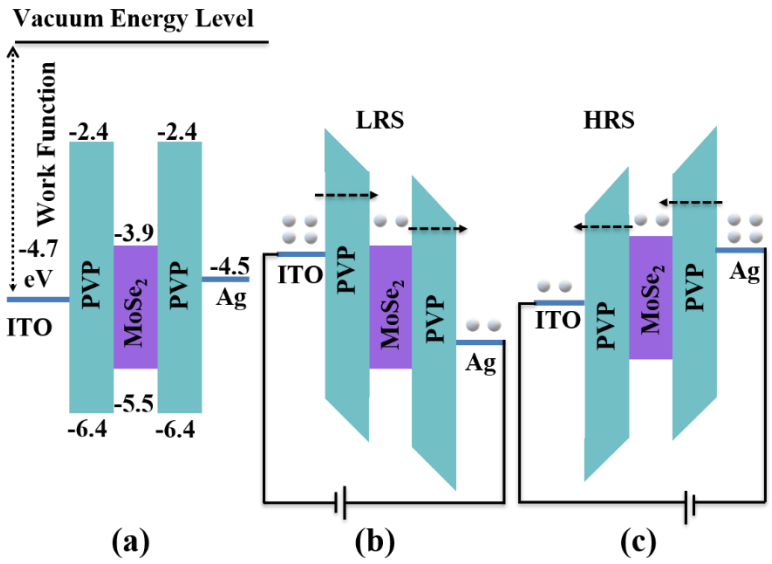


Figure 6.9 Schematic band diagram of Ag/PVP:$MoSe_2$/ITO flexible RRAM device at zero bias **(a).** Charge transport mechanism at LRS at positive voltage **(b),** and HRS at negative voltage **(c).**

6.3.5 Reliability Test

Furthermore, cycle-to-cycle variation in current and voltage was studied to check the reliability of the device. The Weibull distribution is among the widely accepted statistical tools for studying the cycle-to-cycle variability of both current (LRS and HRS) and voltage (SET and RESET), as shown in Figure 6.10. The distribution is plotted with the values obtained from 100 µA compliance condition switching. The LRS and HRS current distributions for more than 1000 cycles are shown in Figure 6.10(a) and (b), respectively. The mean values of LRS and HRS currents were 6.8×10^{-5} A and 5×10^{-7} A, respectively. The Weibull plot for voltage distribution is plotted in Figure 6.10(c) for SET and Figure 6.10(d) for RESET. The mean and shape factor (β) values for SET/RESET voltages are 0.84 V/1.45 V and 10/8.4, respectively, where a higher shape factor is desirable, as it indicates lower variation.

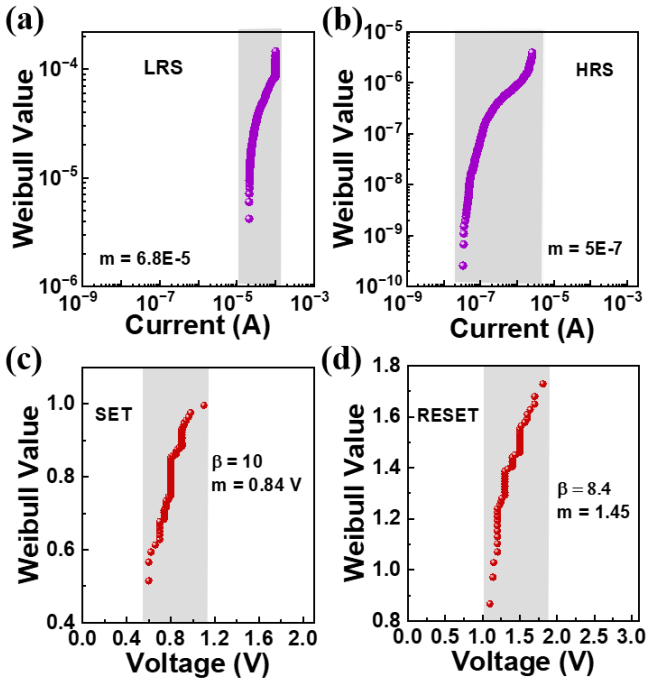


Figure 6.10 Weibull plot of positive current (LRS) **(a),** negative current (HRS) **(b),** SET voltage **(c),** and RESET voltage **(d).**

The variation coefficient of 1000 positive and negative consecutive cycles are 36% and 58%, indicating the probability of 6.8 × 10^{-5} A and 5 × 10^{-7} A, occurring as LRS and HRS currents, respectively, at a read voltage of 0.2 V. It also shows the reliability of the device.

6.3.6 Bending Stability

A major parameter for the evaluation of a flexible electronic device is its ability to maintain its performance during or after mechanical stress (bending). The effect of bending at different radii for studying the mechanical stability of the device is shown in Figure 6.11.

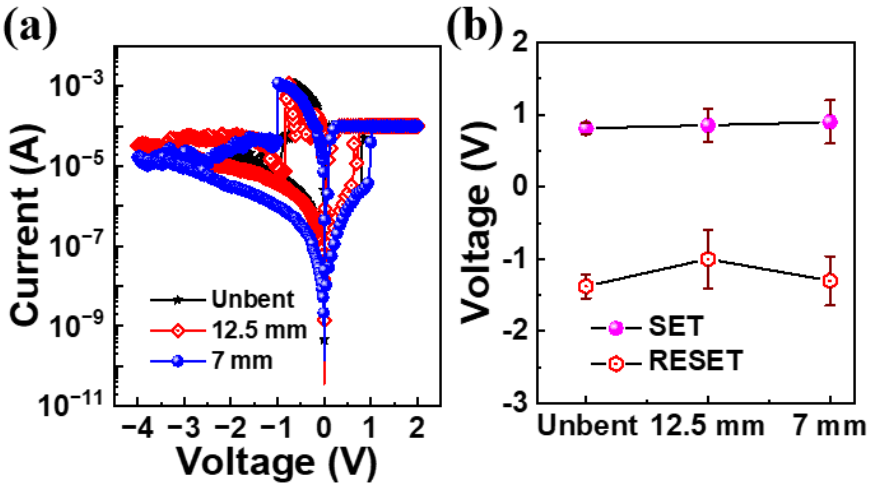


Figure 6. 11 ***I–V*** characteristics **(a)** and an average of SET and RESET voltages **(b)** for unbent and 12.5 mm, and 7 mm bending radii.

The *I–V* characteristics for the unbent condition and for bending at two different radii of 12.5 and 7 mm are shown in Figure 6.11(a). The average of SET and RESET voltages for 100 cycles at each bending radius are shown in Figure 6.11(b). The plot of the mean of SET voltages is

approximately a straight line, indicating negligible variation upon bending. On the other hand, the RESET voltage distribution shows a little variation of less than 0.4 V. A common behavior that can be observed from this plot is that the deviation at a given bending radii has increased compared to the unbent state, and it may be due to the development of cracks in the device during bending. Overall, these results indicate that I_{ON}/I_{OFF} ratios and the SET/RESET voltages are fairly maintained by the device after bending.

The summary of performance parameters of some previously reported RRAM devices with $MoSe_2$ in pristine, composite, or bilayer structures on rigid and flexible substrates is shown in Table 6.2. From this table, it can be observed that the performance of flexible RRAM devices reported by us in this paper is either better than or comparable to most of the previously reported devices in terms of SET/RESET voltages (0.7 V/–1 V), I_{ON}/I_{OFF} (~10^3), and endurance behavior (more than 1000 cycles). Moreover, the Ag/PVP:$MoSe_2$/ITO flexible RRAM devices reported here exhibit a multibit data storage capability (2-bit), stable data retention (10^4 seconds), and good electromechanical stability (bending up to ~7 mm). These desirable properties make the PVP:$MoSe_2$ composite a suitable resistive switching layer candidate for flexible electronics.

Table 6.2: Summary of Performance Parameters of Some Previously Reported RRAM Devices with $MoSe_2$ in Pristine, Composite, or Bilayer.

Device Structure	Substrate	V_{SET} / V_{RESET} (V)	I_{ON}/I_{OFF}	*Endur. Cycles*	Ret. (s)	Year	Ref
Ag/$MoSe_2$/Au	Rigid	2.6/-3	50	100	-	2015	[Yan et al., 2015]
Ag/$MoSe_2$/FTO	Rigid	2.8/-2.2	12	50	-	2016	[Zhang et al., 2016]
Ag/$MoSe_2$/TiO_2/FTO	Rigid	2.2/-1.9	-	50	-	2016	[Han et al., 2016]
Ag/$MoSe_2$/Bi_2Se_3/PMMA/ITO	Rigid	1.9/2.39	10^4 -10^2	10^3	10^6	2019	[Wang et al., 2019]
Cu/$MoSe_2$/PMMA/Ag	Rigid	1/-3	240	300	10^4	2022	[Jian et al., 2022]
Ag/$MoSe_2$/PVA/FTO	Rigid	1/-1	<10	100	2 ×10^2	2022	[Kaur et al., 2022]
Cu/TiO_2/$MoSe_2$/Pt	Rigid	0.4/-0.5	10^2	100	10^3	2023	[Shen et al., 2023]
Ag/$MoSe_2$/ITO	Flexible	1/-1	10^2	120	10^4	2023	[Saini et al., 2023]
Ag/PVP:$MoSe_2$/ITO	Flexible	0.7/-1	10^3	1150	10^4	2024	[Saini et al., 2024]

6.4 Conclusion

High-performance, forming-free, and flexible Ag/PVP:$MoSe_2$/ITO RRAM devices with multibit data storage capability are demonstrated in this work. The novel composite of PVP and $MoSe_2$ as an active layer has shown a reliable resistive switching behavior with low SET/RESET voltages (0.7 V/~-1 V). Multilevel switching (2-bit storage) with excellent retention of around 10^4 seconds was achieved along with the endurance of more than 1000 cycles, which indicates excellent stability and repeatability with very low current operation, i.e., 100 µA. Weibull's distributions of currents and switching voltages have confirmed that the device has very low cycle-to-cycle variation and thus better reliability. Moreover, these devices have shown high mechanical stability upon bending with up to a 7 mm bending radius. These performance parameters strongly suggest that the PVP:$MoSe_2$ composite can be an excellent choice for an active switching layer in flexible RRAM devices and can be further explored for flexible large-area electronics applications.